

## Collision and attachment behavior between fine cassiterite particles and H<sub>2</sub> bubbles

Liu-yi REN<sup>1</sup>, Yi-min ZHANG<sup>1</sup>, Wen-qing QIN<sup>2</sup>, Shen-xu BAO<sup>1</sup>, Jun WANG<sup>2</sup>

1. College of Resources and Environment Engineering, Wuhan University of Technology, Wuhan 430070, China;

2. School of Minerals Processing and Bioengineering, Central South University, Changsha 410083, China

Received 27 April 2013; accepted 6 September 2013

**Abstract:** Particle–bubble interaction during electro-flotation of cassiterite was investigated by determining the recovery of cassiterite and the collision mechanism of cassiterite particle and H<sub>2</sub> bubble. Flotation tests at different conditions were conducted in a single bubble flotation cell. The recovery of cassiterite was found to be affected by cassiterite particle and bubble size. A matching range, in which the best recovery can be obtained, was found between particle and bubble size. Collision, attachment, and detachment of the particle–bubble were observed and captured by a high-speed camera. Particle–bubble collision and attachment were analyzed with the use of particle–bubble interaction theory to obtain the experimental results. An attachment model was introduced and verified through the photos captured by the high-speed camera. A bridge role was observed between the bubbles and particles. Particle–bubble interaction was found to be affected by bubble size and particle size, which significantly influenced not only the collision and attachment behavior of the particles and bubbles but also the flotation recovery of fine cassiterite particles.

**Key words:** cassiterite; fine particle flotation; particle–bubble interaction; collision and attachment

### 1 Introduction

The study of collision and attachment between solid particles and air bubbles in aqueous solutions is the key to understanding froth flotation. Therefore, considerable attention has been focused on understanding and controlling the interactions between colliding particles and bubbles [1–5]. In water, the interaction between particles and air bubbles is a key element to effectively recover valuable minerals via the flotation process [6]. Bubble–particle interaction involves a number of micro-processes, which can be categorized into collision, attachment, and detachment. However, these micro-processes have not been well understood from a quantitative viewpoint despite recent advancements in this field.

Bubble–particle attachment is strongly controlled by surface properties, which are characterized by surface forces and the thinning and rupture of the water film formed when the bubble and the particle are close to each other. Intermolecular (van der Waals), electrical

(double layer), and hydrophobic forces significantly contribute to the surface force interaction between a hydrophobic particle and a gas bubble; these forces are currently being investigated with technologies such as atomic force microscopy [7–11].

The particles dispersed in the bulk liquid during flotation are captured by rising air bubbles, and these particles and bubbles float together to the surface where they form a froth layer. The particles are mainly hydrophobic, which means air bubble capture is enhanced. However, those particles with less hydrophobicity can be transferred to the froth because they can be entrained as a result of rising bubbles. Some particles may detach from the bubbles once they enter the froth phase [12–14]. Only the hydrophobic particles that adhered to the surface of the air bubbles can be floated. Therefore, the probability of attachment determines the selectivity of flotation, whereas the probability of collision critically determines the recovery of cassiterite. Some of the particles are detached from the surface because of inertia and turbulence in a flotation cell. Attachment and detachment are significantly

**Foundation item:** Project (50774094) supported by the National Natural Science Foundation of China; Project (2011BAB05B01) supported by the National Key Technology Research and Development Program of China; Project (2013M542076) supported by the Postdoctoral Science Foundation of China

**Corresponding author:** Yi-min ZHANG; Tel: +86-13554359698; E-mail: [rly1015@163.com](mailto:rly1015@163.com)

DOI: 10.1016/S1003-6326(14)63091-0

determined by the surface chemistry of the bubbles and particles present in the flotation cell. However, predicting the probabilities of these subprocesses with surface chemistry parameters, such as the contact angle,  $z$ -potential, and Hamaker constant, is difficult [15]. Bubble size significantly affects the fine particle flotation. Some researchers have shown that the low flotation recovery of fine particles is mainly caused by the low probability of bubble–particle collision, which is conversely proportional to bubble size [16,17]. That is, the use of small-sized bubbles can increase the probability of collision and the flotation efficiency of fine particles.

Visualization techniques are becoming increasingly popular to investigate particle–bubble attachment [18–20]. A high-speed camera was used to study particle–bubble attachment in flotation; the method involved photographically recording the entire particle–bubble attachment process [21–25]. Previous studies have focused on the single particle rotation during saltation through high-speed photography [26,27] or photography using a stroboscope [28]. KALE et al [29] presented a method based on laser Doppler system to determine the irregular particle rotation. However, the observations were mainly restricted to qualitative descriptions. Few quantitative experimental studies on single particle–single bubble attachment in flotation have been reported.

In this study, a high-speed imaging photography system was used to obtain the direct quantitative measurements of bubble (produced via electrolysis in an aqueous solution) size and to observe motion and particle–bubble interaction. Detailed measurements of particle–bubble aggregation determined the time of water film thinning to characterize attachment interaction. The models assumed to describe the adhesion ways between particle and bubble were introduced.

## 2 Experimental

### 2.1 Materials

A high-grade cassiterite concentrate was formed by gravity separation of a tin ore, which was obtained from Gaofeng Mining Co., Ltd. in Guangxi Autonomous Region, China. The concentrate was further purified by removal of traces of magnetic impurities with a magnetic separator:  $\text{CaCO}_3$  was removed by addition of a dilute hydrochloric acid solution (concentration of 1%) and stirring for about a week, and  $\text{SiO}_2$  was removed with the use of a shaking table. Chemical analysis of the concentrate sample showed that the final solution contained 94%  $\text{SnO}_2$ , which was considered adequately pure for research purposes.

Salicylhydroxamic acid (SHA) with 99% purity was

obtained from Shanghai Jingchun Reagent Limited Company and was used as a collector. Tributyl phosphate (TBP) was obtained from Changsha and was used as an assistant collector. Other chemicals utilized in the test were also analytically pure. Distilled water was used in the experiments.

Two single bubble electro-flotation tubes were prepared for flotation. Bubble size and the interaction between fine cassiterite particles and  $\text{H}_2$  bubbles were observed.

### 2.2 Bubble and particle preparation

The  $\text{H}_2$  bubbles produced from the cathode were used to carry fine cassiterite particles. Bubble size was controlled by the cathode aperture. The  $\text{O}_2$  bubbles produced by the anode were separated by the PTFE diaphragm and exported from the latex tube connected above the anode. Cassiterite particles with several size fractions were prepared through wet milling and hydraulic graduation. Analysis of the particle size of the sample was conducted on Master sizer 2000 (Malvern/England) instrument to determine the presupposed range of the grain size, the test for each sample was repeated three times. The results are shown in Fig. 1.

### 2.3 Electro-flotation

Electro-flotation experiments were conducted in a modified Hallimond tube (100 mL in volume, Fig. 2). The internal diameter of the tube was 24 mm, and the length of the flotation tube was extended to 231 mm to reduce mechanical entrainment of the particles. Entrainment is the mechanical transport of the concentrate after being caught because of rising flotation bubbles, a phenomenon that causes upward liquid flow. Entrainment becomes a problem as the particle size decreases because of the low sedimentation rate of fine particles.

### 2.4 High-speed camera measurements of particle–bubble interaction

Figure 3 shows flake graphite and millipore filtration, and a steel-wire screen was placed at the corresponding place of the experimental cell before the experiment. The chamber was completely filled with 1%  $\text{Na}_2\text{SO}_4$  solution. Positive and negative electrodes were connected to DC power supply. Then, the computer, hardware, and software of the high-speed camera and the DC power supply were switched on. The position of the experimental cell was adjusted until clear images from the camera were obtained. Bubbles entered the experimental cell during flotation or agitation. These bubbles will then move upward because of buoyancy. The motion and process of particle–bubble collision and attachment were captured by a high-speed camera when

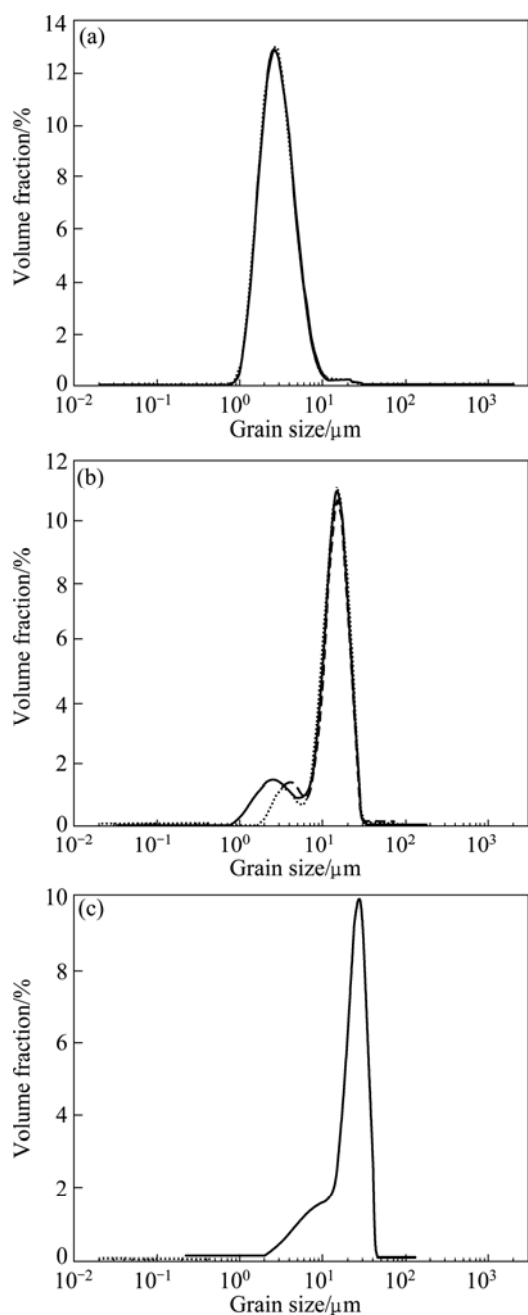


**Fig. 1** Particle size analysis of cassiterite: (a)  $<10 \mu\text{m}$   $\text{SnO}_2$ ; (b)  $10\text{--}20 \mu\text{m}$   $\text{SnO}_2$ ; (c)  $20\text{--}38 \mu\text{m}$   $\text{SnO}_2$

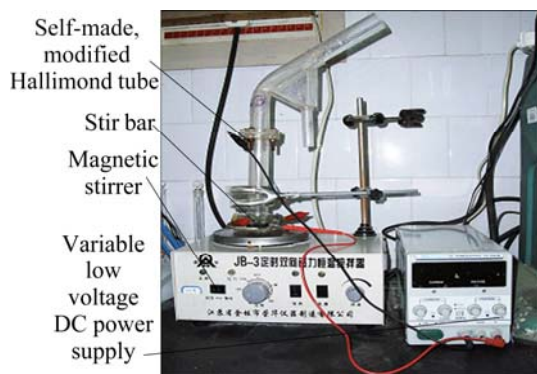


**Fig. 2** Experimental set-up of electro-flotation test

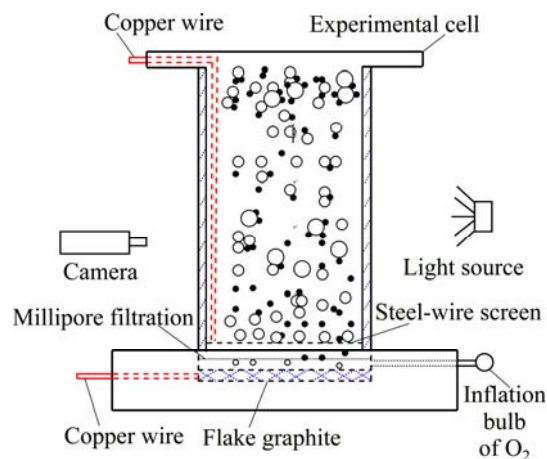


**Fig. 3** Experimental apparatus of high-speed camera measurements

the bubbles passed through the visualization area. The data were then transferred to a PC workstation.

A high-speed camera with a 75 mm lens at F4.5, 2000 f/s shutter speed was used to capture the bubble images. The bubbles were back-illuminated by a 1000 W halogen light that shone on refraction screens located behind the tank and that provided even illumination. The bubble images were directly stored in a computer and were analyzed. Pixel resolution was calibrated by imaging of a ruler located on the plane of the rising bubbles. Analysis of bubble size was conducted with SigmaScan, a commercially developed software program. Results show an average of 12 randomly chosen images captured by the high-speed camera.

### 3 Results and discussion

#### 3.1 Electro-flotation response of cassiterite particles

The average size of the bubbles produced by the different cathode apertures was studied to investigate the flotation behavior of fine cassiterite and the matching relationship between particles and bubbles. Figure 4

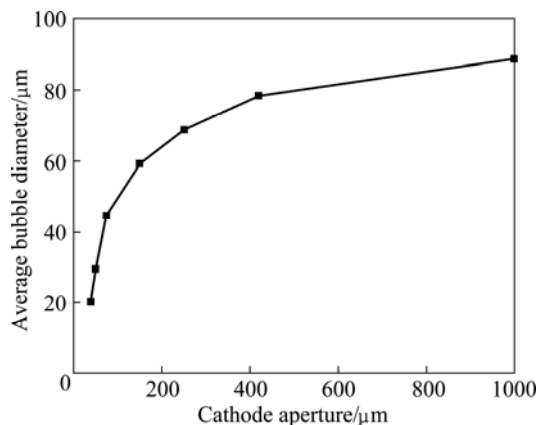


**Fig. 4** Average size of bubbles produced by different cathode apertures

shows the results. Figure 5 presents the relationship between recovery and bubble size (controlled by the cathode apertures) for different particle sizes of cassiterite in the presence of collectors (SHA and TBP).

Figure 4 shows that the average sizes of the bubbles produced by the 38, 50, 74, 150, 250, 420 and 1000  $\mu\text{m}$  cathode apertures are 20.2, 29.5, 44.6, 59.2, 68.7, 78.5, and 88.8  $\mu\text{m}$ , respectively. These data serve as a reference to examine the mutual matching relationship between particle and air bubbles. These results also illustrate that the bubble size increases slightly with an increase in the cathode aperture, but the range decreases when the cathode aperture increases to a certain value.

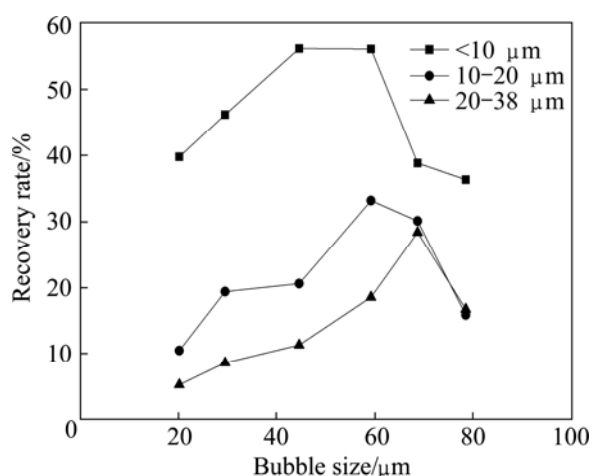


**Fig. 5** Relationship between recovery rate and bubble size for different sizes of cassiterite particles in the presence of SHA at 30 mg/L, pH 6.5 and 1% pulp density

The recovery of cassiterite (<10  $\mu\text{m}$ ) changes sharply as the bubble size increases. The recovery of cassiterite (<10  $\mu\text{m}$ ) is only 39.74% when the bubble size is 20  $\mu\text{m}$ . However, the recovery of cassiterite (<10  $\mu\text{m}$ ) sharply increases to 56.15% when the bubble size is about 45  $\mu\text{m}$ . The recovery of cassiterite (<10  $\mu\text{m}$ ) obviously decreases as the bubble size increases from 59 to 79  $\mu\text{m}$ . The other two size fractions of cassiterite particles demonstrate similar behavior. Figures 4 and 5 show typical results, in which different particle sizes have corresponding bubble sizes: <10, 10–20, and 20–38  $\mu\text{m}$  cassiterite particles match with 44.6, 59.2, and 68.7  $\mu\text{m}$  bubble sizes, respectively. Each particle size fraction of cassiterite corresponds to a certain range of bubble size, in which the highest recovery can be achieved. These experimental results are interpreted by particle–bubble interaction theory. This study demonstrates the advantages of utilizing small bubbles to improve the recovery of fine particles.

### 3.2 Bubble size distribution

The size distribution of the bubble generated from

the cathode under the initial condition was measured with the device shown in Fig. 3. This device is mainly composed of a sampling tube (a viewing chamber) fixed on the test bench. The closed assembly was filled with  $\text{Na}_2\text{SO}_4$  solution similar to that in the flotation cell to limit changes in the bubble environment during sampling. The bubbles rose into the viewing chamber and were captured by the high-speed camera as they collided, attached, and detached with the cassiterite particles or other bubbles. Bubble size was controlled with the use of stainless steel sieves.

The bubble distributions of different planes (front, back, side plane) in the same position were studied, and the results are shown in Figs. 6(a)–(c), respectively, which clearly demonstrate the average size and even distribution of the bubbles. Collision and attachment between bubbles occurred.

### 3.3 Particle–bubble and bubble–bubble collision processes

Particle–bubble collision presumably occurs in the section of the particle surface between angle  $0^\circ$  and the maximum possible collision angle (the theoretical maximum being  $90^\circ$ ) [30]. The bubble size was controlled with a 74  $\mu\text{m}$  cathode aperture. The particle size range was <10  $\mu\text{m}$  in this part. The bubble–particle collision process was studied with the high-speed camera. Bubble–particle and bubble–bubble collisions during the experimental measurements were captured at different times (Fig. 7).

The round objects in Fig. 7 are  $\text{H}_2$  bubbles, whereas the irregular objects are cassiterite particles. The three obvious bubbles labeled 1, 2, and 3 were tracked within a short time and represented the changes in the shape and size of the bubbles and the particle–bubble collision process. The first sample of photos displayed at 1.085 s (Fig. 7(a)) shows that the three bubbles are self-existent, the particles are evenly scattered in the solution, and a few particles adhered on bubbles 1 and 3. Figure 7(b) shows that the collision between bubbles 1 and 3 occurred at 1.1425 s, and additional particles adhered to the three bubbles. Figures 7(c)–(e) show the attachment and merging of the bubbles. However, the merging of the bubbles was not completed, as indicated by Figs. 7(f)–(h). The reasons can be summarized as follows. First, bubble velocity affects the attachment and merging of bubbles. The velocities of bubbles 1 and 3 are different, as indicated by the changes in position of these bubbles. The velocity of bubble 1 is higher than bubble 3 in the beginning at 1.085 s, but that of bubble 3 becomes higher than bubble 1 from 1.36 to 1.475 s. Bubble velocity is affected by the bubble size. The velocity of the small bubble in this study is higher

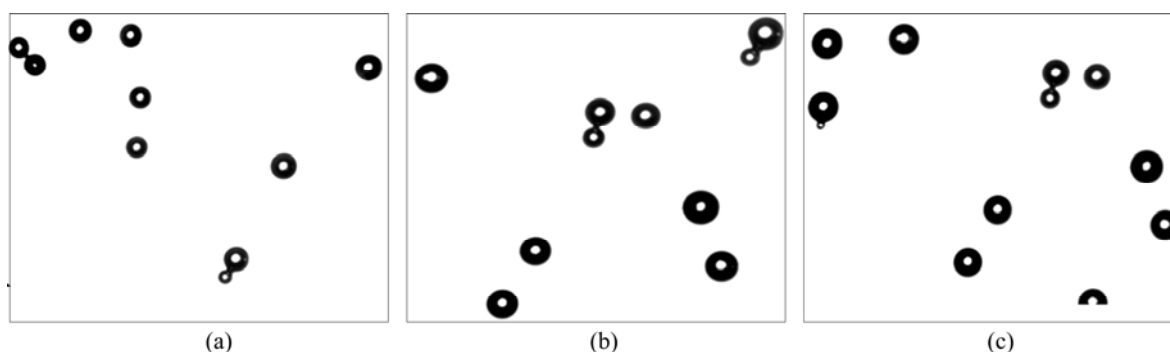


Fig. 6 Bubble distribution in different planes: (a) Front plane; (b) Back plane; (c) Side plane

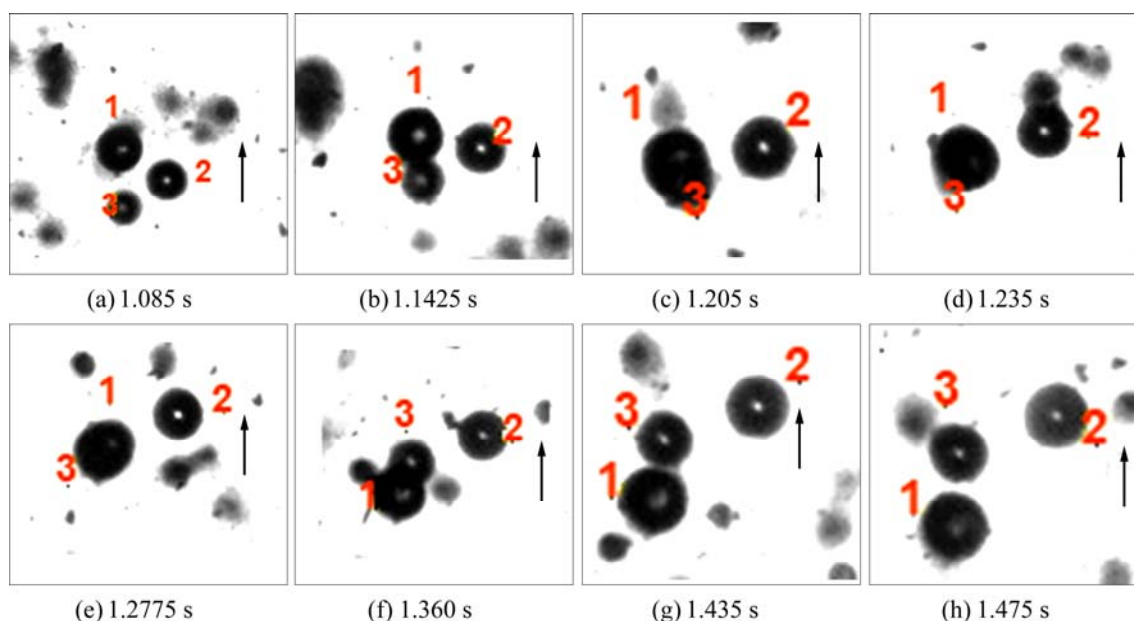


Fig. 7 Collision, adhesion and detachment between bubbles adhered to cassiterite particles at different counting times

than that of the large bubble. Second, bubble property is another important factor that affects the attachment and merging of bubbles. The properties of the particles that adhered to the bubbles, such as quantity and size, are different. The large particles are likely to be captured by large bubbles, whereas the small particles are likely to be captured by the corresponding small bubbles. This leads to the large difference between bubbles.

### 3.4 Particle–bubble attachment

RALSTON et al [31] examined the bubble–particle attachment and detachment in flotation. Zones of particles, film drainage, forces between the bubble and the particle, and the three-phase line of the contact (TPLC) significantly affect the bubble–particle attachment. 0.05 g of cassiterite particles with size of 10  $\mu\text{m}$ , 1%  $\text{Na}_2\text{SO}_4$  solution, and the collectors SHA and TBP were added in a 50 mL beaker and stirred for 5 min. The solution was then transferred into the experimental apparatus with the high-speed camera. Bubble size was

controlled by a stainless steel sieve with 74  $\mu\text{m}$  aperture. Particle–bubble attachment was observed and captured by the high-speed camera. Particle–bubble attachment can be observed clearly in the following samples (Fig. 8).

Ten bubbles were numbered and used as the research objects. Some bubbles that adhered to the cassiterite particles were steady from beginning to end, except for bubble 7, which was detached from the particle in the rising process. However, there was another new bubble adhered to the steady particle–bubble aggregation in this process. Large air bubbles in the flotation cell can easily load the aggregates created by the electro-flotation cell. The attachment process can be observed clearly from bubbles 8, 9, and 10. The aggregate of bubbles on the right side of bubbles 8, 9, and 10 is shown in Fig. 8(e) and the existence of a bridge role is evident. Particles under collector action assume a bridge role, resulting in bubble attachment. The aggregates of the bubbles exist steadily because the liquid film is stable and completely saturates the solid

film. The Hamaker constant is negative, and the corresponding van der Waals force is repulsive to the cassiterite/water/air triple layer when an air bubble approaches a clean cassiterite surface immersed in  $\text{Na}_2\text{SO}_4$  solution. The thin film of an unstable film must be drained and ruptured to enable the resulting TPLC (vapor–water–solid) to expand and form a wetting perimeter before the particle can adhere to the bubble. As a result, the particle and bubble collide and detach. For example, bubbles 8, 9, and 10 separate finally, as shown in Fig. 8(a). Each of these events has an associated characteristic time, whose sum must be less than the contact time between the bubble and the particle to allow flotation to occur. The contact time is generally in the order of  $10^{-2}$ s or less.

### 3.5 Possible particle–bubble attachment models

This study demonstrated the advantages of using the electro-flotation apparatus to examine the aggregation of

hydrophobic fine particles, which is a basic step for the successful flotation of fine particles. The probable mechanism involved can be explained as follows.

First, the flotation particles formed in the electro-flotation apparatus increase the probability of collision with the bubbles in the flotation cell because of flocculation and thus result in a high probability of bubble capture (see Fig. 9(a)). Second, the tiny bubbles formed in the electro-flotation apparatus may cause coalescence from the bubble-bridging mechanism and then increase the apparent particle size. Such an increase enhances the probability of collision with the bubbles in the flotation cell (see Fig. 9(b)). Third, fine bubbles may combine to form flotation-sized bubbles and thus increase the probability of particle–bubble collision (see Fig. 9(c)). Finally, particles frosted with tiny bubbles may combine to form a cluster that is favorable to the attachment of flotation-sized bubbles after the two-stage attachment mechanism (see Figs. 9(d), (e)).

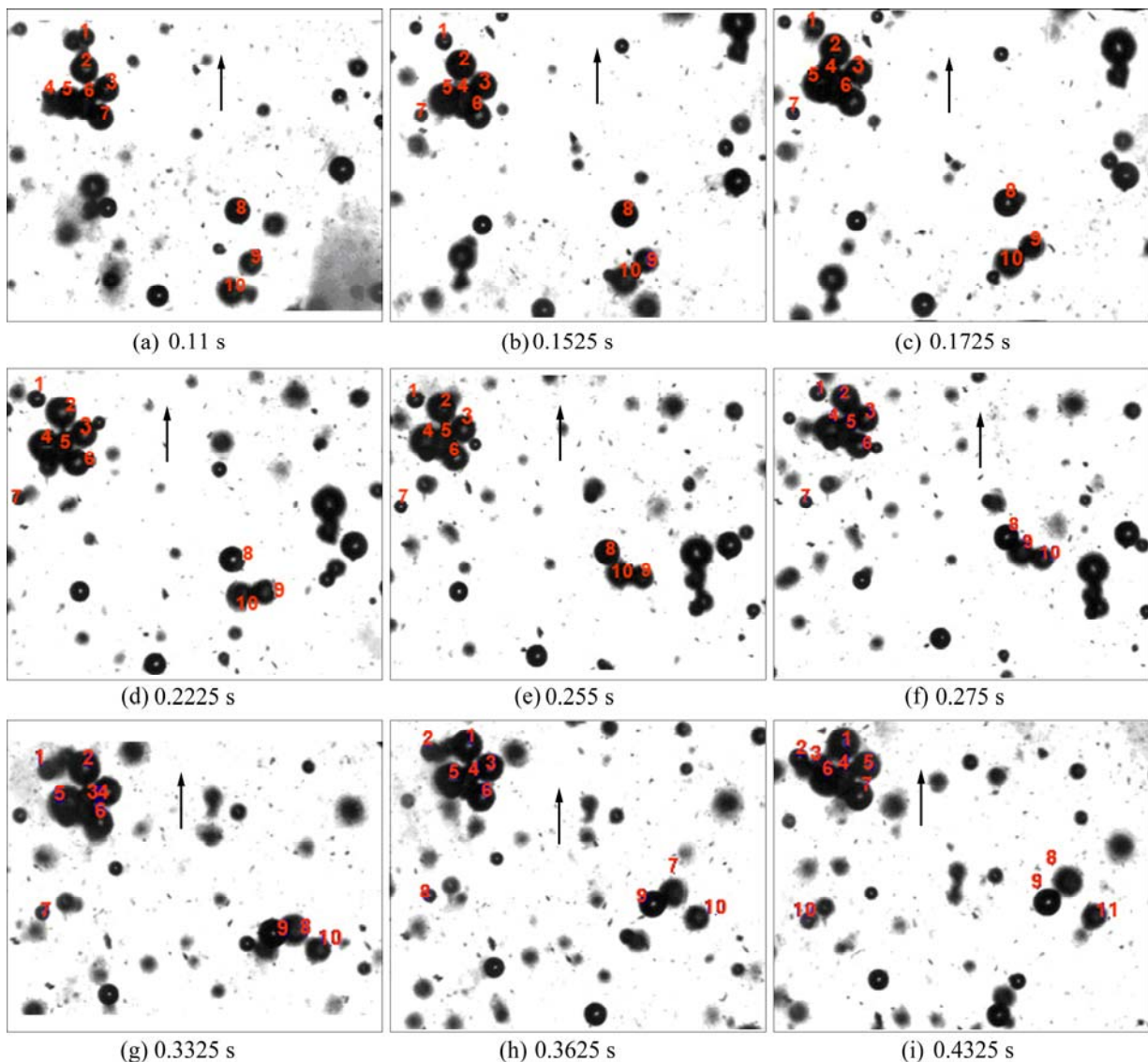
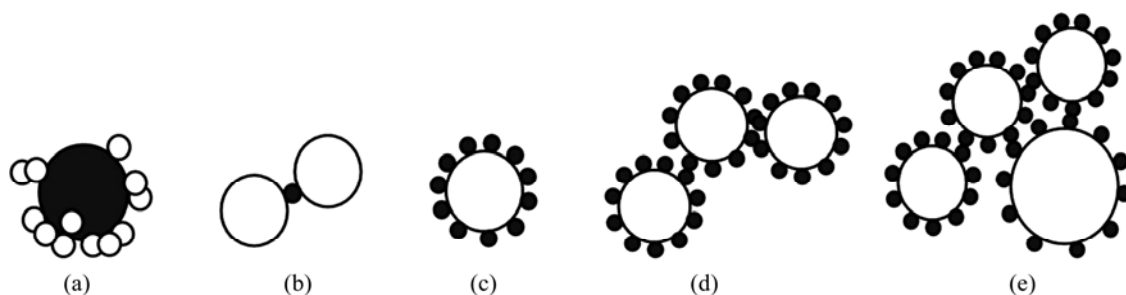


Fig. 8 Adhesion and detachment of bubbles adhered to cassiterite particles displayed at different times



**Fig. 9** Possible particle–bubble adhesion models: (a) Flocculation; (b) Coalescence; (c) Flotation bubble adhesion; (d) Aggregation; (e) Two stage aggregation

The formation of these five models is related to the electro-flotation environment. Various elements, such as the electrolyte concentration, the property and concentration of the collector, and pH value, can affect mineral surface wettability and the surface electrical potential of the particle and bubble. As a result, different attachment models are formed between the particle and bubble. These models may exist together or alone in the same flotation system, but determining which model is dominant is difficult.

#### 4 Conclusions

1) The recovery of cassiterite is affected by particle size and bubble size in electro-flotation experiments. A matching range, in which the best recovery can be obtained, was found between different particle sizes and bubble sizes, <10, 10–20, and 20–38  $\mu\text{m}$  of cassiterite particle sizes match with 45, 59, and 68  $\mu\text{m}$  bubble sizes.

2) The bubbles generated from the cathode are evenly distributed. The collision and attachment between bubbles occur in 1%  $\text{Na}_2\text{SO}_4$  solution without collectors and cassiterite particles. A bridge role was found between bubbles and particles.

3) Particle–bubble attachment models were presented to characterize particle–bubble attachment. Understanding and controlling the interactions between colliding particles and bubbles, including collision, attachment, and detachment, is the key to improving the fine particle flotation.

#### References

- [1] NGUYEN A V, EVANS G M. Attachment interaction between air bubbles and particles in froth flotation [J]. *Exp Therm Fluid Sci*, 2004, 28(5): 381–385.
- [2] NGUYEN A V, NALASKOWSKI J, MILLER J D. A study of bubble-particle interaction using atomic force microscopy [J]. *Miner Eng*, 2003, 16(11): 1173–1181.
- [3] PHAN C M, NGUYEN A V, MILLER J D, EVANS G M, JAMESON G J. Investigations of bubble-particle interactions [J]. *Int J Miner Process*, 2003, 72(1–4): 239–254.
- [4] RALSTON J, DUKHIN S S. The interaction between particles and bubbles [J]. *Colloids Surf A*, 1999, 151(1–2): 3–14.
- [5] QIN Wen-qing, REN Liu-yi, WANG Pei-pei, YANG Cong-ren, ZHANG Yan-sheng. Electro-flotation and collision-attachment mechanism of fine cassiterite [J]. *Transactions of Nonferrous Metals Society of China*, 2012, 22(4): 1711–1717.
- [6] QIN W, REN L, SUN W. Electro-flotation research on fine cassiterite [C]//XXV International Mineral Processing Congress 2010 Proceedings. Brisbane, Queensland, Australia: AusIMM, 2010: 2245–2253.
- [7] ASSEMI S, NGUYEN A V, MILLER J D. Direct measurement of particle–bubble interaction forces using atomic force microscopy [J]. *Int J Miner Process*, 2008, 89(1–4): 65–70.
- [8] DUCKER W A, XU Z, ISRAELACHVILI J N. Measurements of hydrophobic and DLVO forces in bubble–surface interactions in aqueous solutions [J]. *Langmuir*, 1994, 10: 3279–3289.
- [9] FIELDEN M L, HAYES R A, RALSTON J. Surface and capillary forces affecting air bubble–particle interactions in aqueous electrolyte [J]. *Langmuir*, 1996, 12: 3721–3727.
- [10] PREUSS M, BUTT H J. Direct measurement of forces between particles and bubbles [J]. *Int J Miner Process*, 1999, 56(1–4): 99–115.
- [11] SHAHBAZI B, REZAI B, KOLEINI S M J. Bubble–particle collision and attachment probability on fine particles flotation [J]. *Chem Eng Process*, 2010, 49(6): 622–627.
- [12] ROSS V E. An investigation of sub-processes in equilibrium froths. 1. The mechanisms of detachment and drainage [J]. *Int J Miner Process*, 1991, 31(1–2): 37–50.
- [13] ROSS V E. Particle–bubble attachment in flotation froths [J]. *Miner Eng*, 1997, 10(7): 695–706.
- [14] SPYRIDOPOULOS M T, SIMONS S J R. Direct measurement of bubble–particle adhesion forces on the effects of particle hydrophobicity and surfactants [J]. *Chem Eng Res Des A*, 2004, 82(4): 490–498.
- [15] YOON R H. The role of hydrodynamic and surface forces in bubble-particle interaction [J]. *Int J Miner Process*, 2000, 58(1–4): 129–143.
- [16] AHMED N, JAMESON G J. The effect of bubble size on the rate of flotation of fine particles [J]. *Int J Miner Process*, 1985, 14(3): 195–215.
- [17] SUN W, HU Y H, DAI J P, LIU R Q. Observation of fine particle aggregating behavior induced by high intensity conditioning using high speed CCD [J]. *Transactions of Nonferrous Metals Society of China*, 2006, 16(1): 198–202.
- [18] DAVES A P H, ROSSI L, DUKE S R. A method for visualization and measurement of ink adsorption rates at bubble surfaces [J]. *AIChE Symp Ser*, 2000, 324: 96–105.
- [19] WANG W X, ZHOU Z A, NANDAKUMAR K, XU Z H, MASLIYAH J H. Attachment of individual particles to a stationary air bubble in model systems [J]. *Int J Miner Process*, 2003, 68(1–4):

- 47–69.
- [20] ZHOU Z A, XU Z, MASLIYAH J, KASONGO T, KIZOR T, COX D. Application of on-line visualization to flotation systems [C]//Proceedings of the 32nd Annual Meeting of the Canadian Mineral Processors. Ottawa: CIM, 2000: 120–137.
- [21] CHEN H, LI X J, WAN M X, WANG S P. High-speed observation of cavitation bubble cloud structures in the focal region of a 1.2 MHz high-intensity focused ultrasound transducer [J]. *Ultrason Sonochem*, 2007, 14(3): 291–297.
- [22] LUKE A, CHENG D C. High speed video recording of bubble formation with pool boiling [J]. *International Journal of Thermal Sciences*, 2006, 45(3): 310–320.
- [23] SAKAKIBARA K, YAMADA M, MIYAMOTO Y, SAITO T. Measurement of the surrounding liquid motion of a single rising bubble using a Dual-Camera PIV system [J]. *Flow Measurement and Instrumentation*, 2007, 18(5–6): 211–215.
- [24] SIEDEL S, CIOULACHTJIAN S, BONJOUR J. Experimental analysis of bubble growth, departure and interactions during pool boiling on artificial nucleation sites [J]. *Experimental Thermal and Fluid Science*, 2008, 32(8): 1504–1511.
- [25] WU X C, WANG Q H, LUO Z Y, FANG M X, CEN K F. Experimental study of particle rotation characteristics with high-speed digital imaging system [J]. *Powder Technol*, 2008, 181(1): 21–30.
- [26] TSUJI Y, MORKAWA Y, MIZUMO O. Experimental measurement of the Magnus force on a rotating sphere at low Reynolds numbers [J]. *Journal of Fluids Engineering*, 1985, 107: 484–488.
- [27] WHITE B R. Two-phase measurements of saltating turbulent boundary layer flow [J]. *Int J Multiphase Flow*, 1982, 8: 459–473.
- [28] LEE H Y, HSU I S. Particle spinning motion during saltating process [J]. *Journal of Hydraulic Engineering*, 1996, 122: 587–590.
- [29] KALE S R, RAMEZAN M, ANDERSON R J. Measurement of particle rotational velocity using a laser anemometer [J]. *Particle and Particle Systems Characterization*, 1989, 6: 59–63.
- [30] BASAROVA P, MACHON V, HUBICKA M, HORN D. Collision processes involving a single rising bubble and a larger stationary spherical particle [J]. *Int J Miner Process*, 2010, 94(1–2): 58–66.
- [31] RALSTON J, FORNASIERO D, HAYES R. Bubble-particle attachment and detachment in flotation [J]. *Int J Miner Process*, 1999, 56(1–4): 133–164.

## 锡石颗粒与氢气泡间的碰撞粘附行为

任浏祎<sup>1</sup>, 张一敏<sup>1</sup>, 覃文庆<sup>2</sup>, 包申旭<sup>1</sup>, 王军<sup>2</sup>

1. 武汉理工大学 资源与环境工程学院, 武汉 430070;

2. 中南大学 资源加工与生物工程学院, 长沙 410083

**摘要:** 运用回收率和细粒锡石-气泡间的碰撞机制研究颗粒-气泡间的相互作用。用单泡浮选管进行浮选实验, 考查不同条件下细粒锡石的浮选行为。结果表明, 浮选回收率受颗粒和气泡尺寸的影响很大, 在浮选回收率最高时, 颗粒和气泡间存在一个最佳的匹配范围。运用高速摄影仪观察并捕捉颗粒-气泡间的碰撞、粘附、脱附过程, 在已有理论的基础上, 分析颗粒-气泡间的碰撞-粘附现象并解释浮选实验结果, 通过捕捉图片证明颗粒-气泡间的粘附模型, 发现颗粒-气泡间的桥连作用。锡石、气泡尺寸的大小影响锡石-气泡间的相互作用, 这不仅影响锡石-气泡间的碰撞粘附行为, 并最终影响细粒锡石的浮选回收率。

**关键词:** 锡石; 细粒浮选; 颗粒-气泡间相互作用; 碰撞粘附

(Edited by Xiang-qun LI)